Radar interferometry for measuring tidal strains across cracks on Europa

David Sandwell,[1] Paul Rosen,[2] William Moore,[3] and Eric Gurrola[2]

Received 8 April 2004; revised 26 June 2004; accepted 21 July 2004; published 16 November 2004.

[1] A major uncertainty in understanding the interaction between the surface of Europa and its ocean below is the present-day activity of fractures. Using well-constrained models for tidal strain and a force balance in a cracked shell, we estimate the shear and normal displacement of cracks that penetrate upward from the base of the shell. If more than half of the plate is fractured, then surface displacements having amplitudes of 3 to 30 cm will be localized in a band 1 to 100 km from the crack. Plate spreading will occur if more than ~85% of the plate is fractured. The pattern of deformation is sensitive to both the percentage of plate that is cracked and the total thickness of the shell. Repeat-pass radar interferometry could easily detect and map the activity of the cracks during a short experiment from a variety of suitable orbits with repeating ground tracks. *INDEX TERMS:* 1227 Geodesy and Gravity: Planetary geodesy and gravity (5420, 5714, 6019); 1241 Geodesy and Gravity: Satellite orbits; 5475 Planetology: Solid Surface Planets: Tectonics (8149); 5494 Planetology: Solid Surface Planets: Instruments and techniques; *KEYWORDS:* crack, Europa, interferometry

Citation: Sandwell, D., P. Rosen, W. Moore, and E. Gurrola (2004), Radar interferometry for measuring tidal strains across cracks on Europa, *J. Geophys. Res.*, *109*, E11003, doi:10.1029/2004JE002276.

1. Introduction

[2] A major step in determining the prospects for finding evidence of life on Europa is establishing the minimum thickness of the ice shell and determining if cracks in the shell penetrate its entire thickness. Galileo spacecraft magnetometer data indicate a near-surface conductive layer [*Kivelson et al.*, 2000] suggesting that a liquid ocean lies beneath an ice shell. Moreover, there is surface morphological evidence for once mobile ''icebergs,'' suggesting that the liquid ocean has been exposed at the surface and the plate has been relatively thin (~2 km) [*Carr et al.*, 1998]. However, the present-day average shell thickness is still poorly constrained. Estimates of the asymptotic thickness vary from 3 km for a thin brittle shell [*Greenberg et al.*, 1998] to 6–18 km for a convecting layer with high heat production from the silicate mantle [*Buck et al.*, 2002] to 30 km for lower internal heat generation [*Ojakangas and Stevenson*, 1989]. Flexure models also predict a range of shell thicknesses of 3 to 15 km [*Figueredo et al.*, 2002; *Nimmo et al.*, 2003]. All of these estimates, however, are strongly model dependent, in particular relying on assumptions regarding heat transport and heat production in the shell and the deep interior of Europa.

[3] Linear and cycloidal ridges, which are pervasive across the surface of Europa, are believed to form above cracks in the icy shell [*Greeley et al.*, 2004; *Hoppa et al.*, 1999b]. The detailed morphology of the ridges is suggestive of both tensional deformation [*Greeley et al.*, 2004; *Greenberg et al.*, 1998; *Prockter et al.*, 2002] and shear deformation [*Hoppa et al.*, 1999a]; they are especially prevalent at low latitudes [*Michalski and Greeley*, 2002]. There is still debate on whether the cracks form in response to diurnal tidal strains and/or asynchronous rotation of the shell across the permanent tidal bulge [*Geissler et al.*, 1998; *Greenberg et al.*, 1998]. Linear ridges crisscross the surface revealing stratigraphic relationships and a variety of morphologic characteristics [*Carr et al.*, 1998; *Greenberg et al.*, 1998]. Simple models suggest the youngest ridges are more than 30,000 years old [*Greenberg et al.*, 1998], while crater density suggests that the average of the surface must be younger than about 50 Myr [*Greeley et al.*, 2004].

[4] One of the major uncertainties in the formation of these ridges is the depth and extent of cracking. *Greenberg et al.* [1998, 2002] suggest that they penetrate through the entire shell thickness and pump water to the surface on every tidal cycle. *Prockter et al.* [2002] suggest they are analogous to seafloor spreading ridges. In this model, melt is delivered to a shallow magma chamber where is freezes; opening of the rift is accommodated by brittle fracture/normal faults in the upper part of the plate and ductile flow in the lower part of the plate. This seafloor spreading-type model does not bring water closer than about 2 km to the surface. The differences between these end-member models have important implications for the prospect of detecting life on Europa and also have significant implications for the tectonic evolution of Europa's icy shell.

[5] Experiments have been proposed to help discriminate among the various models of shell thickness and cracking/rifting including landing a seismometer on Europa [*Lee et*

[1]Scripps Institution of Oceanography, La Jolla, California, USA.
[2]Jet Propulsion Laboratory, California Institute of Technology, Pasadena, California, USA.
[3]Department of Earth and Space Sciences, University of California, Los Angeles, California, USA.

0148-0227/04/2004JE002276$09.00

al., 2003; *Moore and Makris*, 2003] radio echo sounding [*Blankenship et al.*, 2003]; infrared imaging [*Blaney and Spencer*, 2003] and magnetotellurics [*Khurana et al.*, 2003]. The seismic method could provide definitive estimates of plate thickness and the depth distribution of seismically active cracks but landing an instrument on the surface is both challenging and expensive.

[6] Here we investigate the feasibility of using repeat-pass synthetic aperture radar interferometry (InSAR) for estimating both the plate thickness and the depth distribution of cracking in a future orbital mission at Europa (R. Greeley et al., Report of the NASA Science Definition Team for the Jupiter Icy Moons Orbiter, http://ossim.hq.nasa.gov/jimo/, National Aeronautics and Space Administration, Washington, D. C., 2004). On Earth, InSAR has provided mm-precision deformation measurements (over 100-km wide swaths) associated with earthquakes, volcanic inflation, groundwater movements, and motion of ice due to tides and streams [*Massonnet and Feigl*, 1998; *Rosen et al.*, 2000]. We first show that the global strain due to diurnal tides [*Greenberg et al.*, 1998; *Moore and Schubert*, 2000] will be amplified in areas where cracks penetrate a significant fraction of the shell thickness. The strain concentration above a crack is converted to the equivalent displacement on a fracture at depth. We then compute a suite of dislocation models to establish the set that could be easily detected by InSAR. We further explore the radar and orbital characteristics that best resolve these differences in plate thickness and crack extent. If the crack penetrates less than half the plate thickness, then no signal will be detected above the noise level of the radar interferogram. However, even a negative observation has important implications for present-day exchange of water with the surface of Europa.

2. Amplification of Tidal Strains Above Linear Cracks

[7] Cracks and ridges observed on Europa are typically greater than 100 km long and are pervasive especially in the equatorial regions where tide models predict maximum strain [*Greeley et al.*, 2004; *Greenberg et al.*, 1998; *Hoppa et al.*, 1999b]. Using a simple force balance in a thin elastic shell, we calculate the amplification of the tidal strain above a crack that penetrates part of the way through the shell. Initially we will consider cracks that are much longer than the range of proposed shell thicknesses (3–30 km). Tide models provide robust estimates of global strain as long as the shell thickness is less than about 30 km [*Moore and Schubert*, 2000]. Consider a crack that penetrates from the base of an elastic plate of thickness H to some depth d as shown in Figure 1. As proposed by *Crawford and Stevenson* [1988] we consider only bottom-up cracks that are filled with water so the walls of the crack are nearly stress-free. While top-down, strike-slip cracks are physically possible, top-down extensional cracks (dry) would require stresses that greatly exceed the tidal stress (~40 kPa). Moreover, at a depth of only a few hundred meters the differential stress would exceed the fracture strength of the ice and the walls of the crack would collapse.

[8] Assuming a bottom-up water-filled crack, the intact plate above the crack must support the same depth-integrated stress (normal or shear) as the uncracked plate. The force balance is

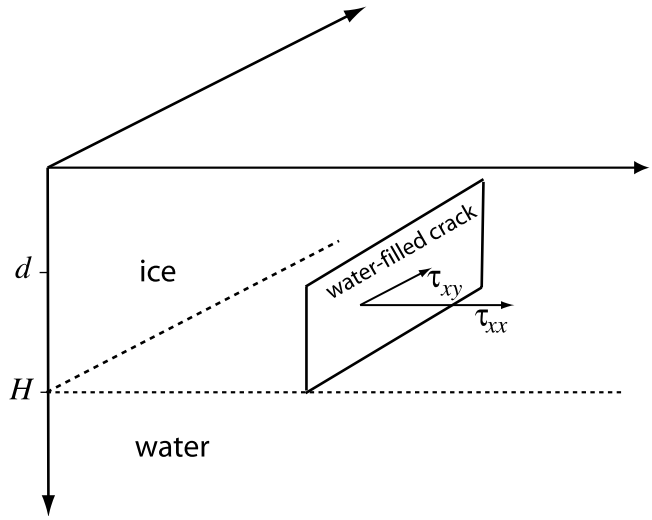

Figure 1. Diagram showing a crack extending from the base of the plate to a variable depth d. Fault-normal extension across the crack can occur only if the void is replaced by high-pressure water, so we expect only bottom-up cracks [*Crawford and Stevenson*, 1988]. In contrast, shear displacement could occur on both shallow and deep fault planes.

$$\int_0^d \tau_c(z)dz = \int_0^H \tau_o dz = H\tau_o, \tag{1}$$

where τ_o is one of the stress components (normal or shear) caused by the global tidal fluctuations. This equation can be written in terms of the depth-averaged stress:

$$\overline{\tau_c} = \frac{H}{d}\tau_o. \tag{2}$$

Thus it is clear that the tidal stress is amplified by the ratio of the plate thickness to crack depth. Next assume the strains are small so stress is linearly related to strain by Hooke's law; equation (2) can be rewritten in terms of strain:

$$\bar{\varepsilon} = \frac{H}{d}\varepsilon_o, \tag{3}$$

where ε_o is one of the components of tidal strain and $\bar{\varepsilon}$ is the depth-averaged strain in the intact layer above the crack. Radar interferometry provides only a local measure of differential displacement so we are only interested in the local strain perturbation $\overline{\Delta\varepsilon}$. The local strain perturbation is the depth-averaged strain minus the large-scale tidal strain or

$$\overline{\Delta\varepsilon} = \varepsilon_o\left(\frac{H}{d} - 1\right). \tag{4}$$

The semidiurnal tides on Europa (1.8-day period) have radial amplitude of ~30 m and are distributed over a distance of 1500 km corresponding to a strain of about 2×10^{-5}; the horizontal strains are 2–3 times smaller. Typical values of horizontal strain for the equatorial regions of Europa are 5×10^{-6} for shear and 8×10^{-6} for dilatation [*Moore and Schubert*, 2000]. A crack that penetrates halfway through the plate will have a local strain perturbation that is equal to the global tidal strain (equation (4)); a higher cracked fraction of 0.9 produces 9 times the global tidal strain. We show below that this local strain perturbation will produce localized surface displacements. The primary issue addressed in this paper is what is the minimum cracked fraction that could be measured in repeat-pass radar interferometry. However, before considering this issue, we provide a plausible upper bound on the cracked fraction.

3. An Upper Bound on the Fraction of Plate Fractured

[9] To develop this upper bound, we will initially assume that the uncracked part of the plate does not undergo complete failure (opening) in response to the extensional tidal force. Complete failure would occur when the depth-integrated tidal stress exceeds the depth-integrated plate strength. As discussed above, the force per length F acting on the shell away from the crack must be equal to the force per unit length transmitted by the intact layer above the crack F_c. This force is related to the strain using the thin elastic plate approximation [*Turcotte and Schubert*, 2002]

$$F_c = F = \frac{HE}{(1-\nu^2)}\varepsilon_o, \tag{5}$$

where Young's modulus E (5 GPa) and ν is Poisson's ratio (0.3). The Young's modulus appropriate for Europa's shell is uncertain and ranges between 1 and 9 GPa. Recent flexure studies, which include the finite yield strength of the plate, suggest the larger value of 9 GPa is more appropriate for ice [*Nimmo*, 2004; *Cole and Durell*, 1995; *Vaughan*, 1995]. Here we have used an intermediate value.

[10] We balance this force with the integrated strength of the plate above the crack assuming the ice fails by sliding on shallow faults. *Byerlee* [1978] showed that the frictional resistance on a fault depends on the fault-normal stress and the coefficient of friction and is largely independent of material properties. Suppose that the brittle layer of ice above the crack has closed fractures oriented in all directions and a differential stress (horizontal - vertical) $\Delta\tau$ is applied. Frictional sliding will occur on optimally-oriented faults when the resolved shear stress exceeds the Byerlee criteria [*Byerlee*, 1978]. The magnitude of this differential stress is called the yield strength [*Brace and Kohlstedt*, 1980] and it is primarily a function of the overburden pressure as follows:

$$\Delta\tau = \begin{cases} 0.7\rho g z & \text{extension} \\ -3\rho g z & \text{compression} \end{cases}, \tag{6}$$

where ρ is the ice density (~920 kg m^{-3}) and g is acceleration of gravity (1.3 m s^{-2}). The integrated strength of the plate in tension is $0.35\rho g d^2$. This strength must exceed the applied tidal force or the crack opening is unbounded. This provides a bound on the depth to the top of the crack:

$$d > \left(\frac{2.9HE\varepsilon_o}{\rho g(1-\nu^2)}\right)^{1/2}. \tag{7}$$

Using values provided above, we find the depth to the top of the crack must be greater than 570 m, 1040 m, and 1800 m for plate thickness of 3 km, 10 km, and 30 km, respectively. In these cases more than 0.8 of the plate is fractured and the strain localization will be more than 4 times the global tidal strain. Of course this is an upper bound on the fraction of plate that is cracked so strain localization could be much lower. Note also that the cracked fraction cannot exceed the ratio of the density of the ice to the density of the water (~0.92) because the water cannot rise above its isostatic level [*Crawford and Stevenson*, 1988]. It is interesting to note that this isostatic bound will override the plate strength bound when the plate thickness exceeds about 10 km.

[11] This analysis suggests that plate spreading will occur when the cracked fraction slightly exceeds the maximum permitted by Byerlee's law. Consider the deformation during a complete tidal cycle. A slight opening of the upper brittle layer will occur during the maximum of the extensional phase of the tide due to the activation of normal faults. However, the layer will not close during the compressional phase because the integrated strength of the plate is 4 times greater in compression than in tension (equation (6)) [*Brace and Kohlstedt*, 1980]. This will lead to plate spreading analogous to the shear walking described by [*Hoppa et al.*, 1999a]. The model provides no estimate of spreading rate, however.

4. Displacement Due to a Vertical Dislocation in an Elastic Plate

[12] The detailed surface displacement due to shear or normal displacement of a crack at depth depends on several parameters including the fraction of the plate that is cracked, the plate thickness, the restoring force of gravity, and whether the crack occurs at the top or bottom of the plate. Closed form analytic solutions have been developed for the surface displacement above a 2-D crack in an elastic plate [*Nur and Mavco*, 1974; *Rybicki*, 1971; *Savage and Prescott*, 1978]. These models provide the displacement, stress, and strain caused by horizontal shear, vertical shear, or fault-normal displacement as a function of depth. Semianalytic methods have been used to extend these solutions to three dimensions [*Rundle and Jackson*, 1977; *Smith and Sandwell*, 2004]. We use the 3-D formulation of Smith and Sandwell (submitted manuscript, 2004) to calculate the surface displacement from a finite-length crack. The important model parameters are Young's modulus (5 GPa), Poisson's ratio (0.3), water density (1000 kg m^{-3}) and acceleration of gravity (1.3 m s^{-2}).

[13] Before we can simulate the surface deformation from a 3-D dislocation model we need to specify the displacement at depth across the crack surface that is consistent with

Table 1. Relation Between Strain Localization and Crack Displacement on Fault[a]

Fraction of Plate Cracked (*H-d*)/*H*	Depth-Averaged Strain $\times 10^{-6}$ (Shear/Normal)	Shear Displacement Needed, m	Normal Displacement Needed, m
0.1	0.55/0.88	0.019	0.042
0.2	1.25/2.00	0.026	0.063
0.3	2.15/3.44	0.033	0.086
0.4	3.35/5.36	0.040	0.112
0.5	5.00/8.00	0.048	0.142
0.6	7.50/12.0	0.057	0.177
0.7	11.7/18.6	0.068	0.221
0.8	20.0/32.0	0.086	0.291
0.9	45.0/72.0	0.129	0.352
0.95	95.0/152.0	0.203	0.451

[a] $H = 10$ km. Values of global tidal strain are 5×10^{-6} for shear and 8×10^{-6} for dilatation [*Moore and Schubert*, 2000].

the depth-integrated strain provided by the tide model. We use a trial approach to relate these two quantities. First we introduce one meter of shear (or fault-normal) displacement on a crack extending from the base of the plate to a uniform depth d and calculate the strain directly above the crack. From numerical integration we find that the depth-averaged strain is about equal to the strain at 0.72 times the crack depth d; this is largely independent of plate thickness or fraction of plate cracked. Using this relationship we adjust the displacement to provide the correct depth-averaged strain (Table 1). For example, if the fraction of plate cracked is 0.9 then the localized depth-averaged extensional strain given by equation (4) is 72×10^{-6}. For plate thicknesses of 3, 10 and 30 km, the normal displacement needed to generate the depth-averaged strain is 0.161, 0.352 and 0.859 m, respectively (Table 1). This amount of displacement is not unreasonably large considering total extensional displacement across the surface of Europa is about 10 m.

[14] To calculate the surface displacement, both shear and normal displacement are applied to a 256-km-long crack in an elastic plate with a range of thicknesses (3 km, 10 km, or 30 km). The shear displacement mainly drives fault-parallel displacement as shown in Figure 2 (top). The amplitude of the displacement depends strongly on the fraction of plate that is cracked. Little displacement occurs until the cracked fraction exceeds 0.5. However, displacement grows rapidly as the cracked fraction exceeds 0.9. Fault-normal displacement on the crack drives both fault-perpendicular displacement and vertical displacement on the surface (Figure 2, middle and bottom). The behavior of the fault-perpendicular displacement is similar to the fault-parallel displacement; the amplitude depends on crack displacement and the width of the displacement pattern is comparable to the plate thickness (10 km for this model).

[15] The amplitude of the vertical displacement also depends on the fraction of plate cracked but in this case the gravity restoring force and flexure are important. Oddly, we find that the amplitude of the vertical displacement is larger than both of the other horizontal components. To understand how vertical deformation is driven by horizontal opening of the crack and why this displacement is large, consider the force balance on the cracked plate as shown in Figure 3. Far from the crack, the center of force acting on the plate is at a depth of $H/2$. Above the crack, the center of

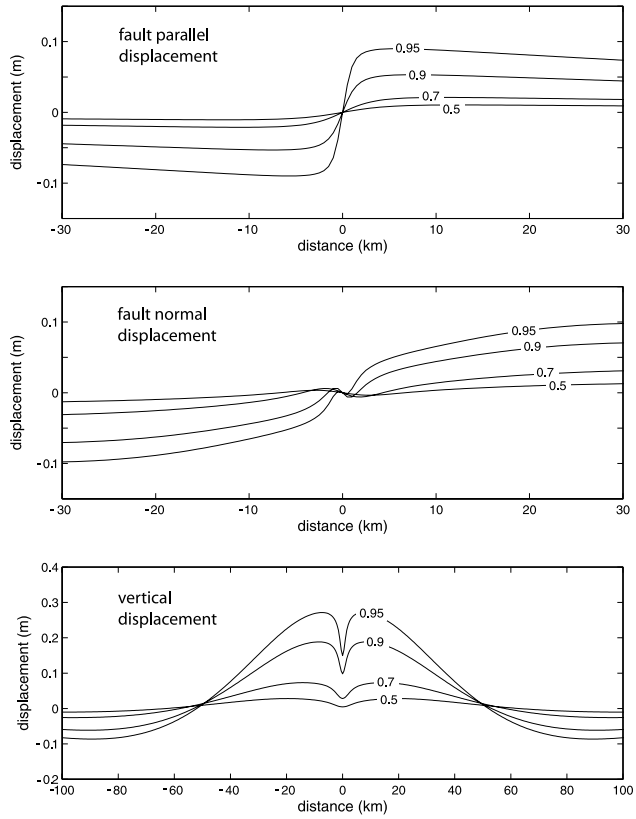

Figure 2. (top) Fault-parallel displacement at the surface caused by strike-slip displacement on a crack extending from the base of a 10-km-thick plate to a variable fraction of the plate thickness (0.5, 0.7, 0.9, and 0.95). The amplitude of the signal grows dramatically as the fraction of plate cracked exceeds 0.5. The width of the deformation pattern is largely controlled by the plate thickness. (middle) Fault-normal displacement at the surface caused by opening of a crack at depth (Table 1). (bottom) Vertical displacement caused by opening of a crack at depth. The width of the deformation pattern is controlled by the flexural wavelength.

force is at a depth of about $d/2$. The difference in these two depths corresponds to a moment arm of length $(H - d)/2$. This bending moment of $F(H - d)/2$ must be balanced by plate flexure. Similar arguments are used to explain the axial valley topography at slow spreading ridges [*Phipps Morgan*, 1987]. The amplitude of the moment grows as the fraction of cracked plate is increased. Also since the strain in the model is prescribed by the tides, the magnitude of the force and thus the amplitude of the bending moment are proportional to the product of plate thickness H and Young's

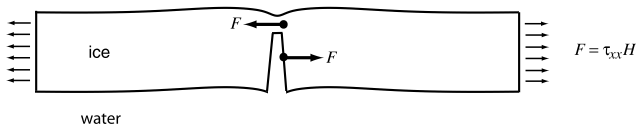

Figure 3. Force balance in a cracked plate under tension.

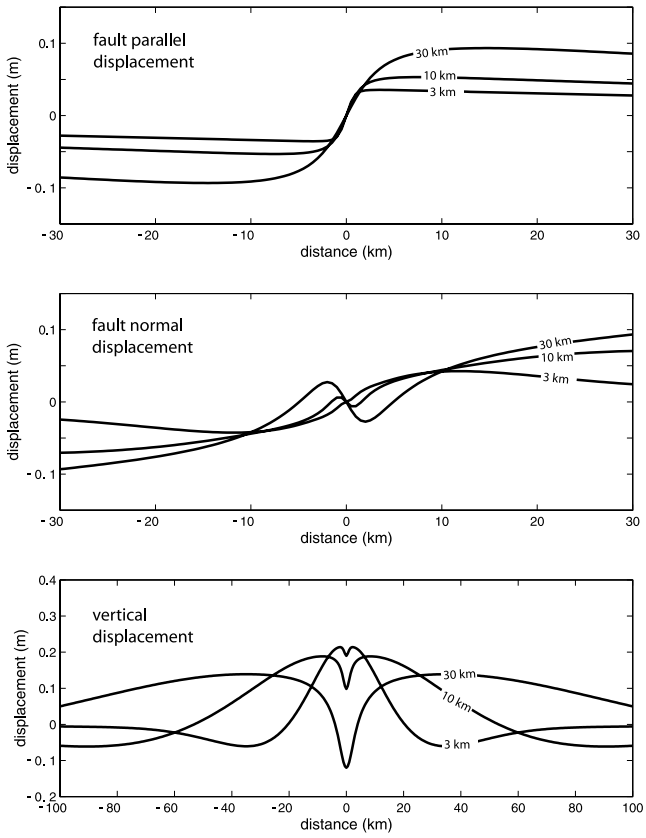

Figure 4. (top) Fault-parallel displacement at the surface caused by shear displacement where the cracked fraction is 0.9 and the plate thickness is varied. The amplitude and width of the displacement grow with increasing plate thickness. (middle) Fault-normal displacement at the surface caused by opening of a crack at depth. (bottom) Vertical displacement caused by opening of a crack at depth. The width of the deformation pattern is controlled by the flexural wavelength, which is a strong function of plate thickness. The shear/normal displacement on the crack for plate thicknesses of 3, 10, and 30 km are 0.082/0.161 m, 0.129/0.352 m, and 0.252/0.859 m, respectively.

modulus, E. An approximate formula for the bending moment when the strain ε_{xx} is prescribed is

$$M = EH\frac{(H-d)}{2}\varepsilon_{xx}. \tag{8}$$

This moment must be balanced by the bending moment of the flexural topography. Note that a thinner plate has a smaller moment than a thicker plate. As noted above, the Young's modulus appropriate for Europa's shell is uncertain and ranges between 1 and 9 GPa. Here we have used an intermediate value of 5 GPa. Since the moment scales linearly with Young's modulus, our models may underestimate the vertical displacement.

[16] Plate thickness also affects the amplitude and shape of the surface displacement. We have explored models with three thicknesses 3, 10, and 30 km, as shown in Figure 4. In these cases the fraction of plate cracked was set to a constant value of 0.9, which is the maximum fraction assuming the ice and water remain in hydrostatic equilibrium [*Crawford and Stevenson*, 1988]. Both the amplitude and width of the fault-parallel deformation (Figure 4, top) increase with increasing plate thickness. A similar relationship occurs with the fault-normal displacement caused by opening of the crack (Figure 4, middle). The vertical deformation is a strong function of plate thickness. For this range of thicknesses, the flexural wavelength varies from 20 km to ~200 km. The downwarping of the plate above the crack is also a strong function of plate thickness. Therefore measurements of vertical displacement with vertical precision better than 0.05 m, horizontal spatial resolution better than 1 km and spatial coverage of about 100 km could be used to identify areas of significant cracking and also estimate the thickness of the elastic plate.

5. Repeat-Pass Radar Interferometry

[17] Synthetic Aperture Radar (SAR) and Interferometric SAR (InSAR) have revolutionized many areas of earth sciences including evaluation of surface and subsurface properties (both geologic and biologic), crustal dynamics, glaciology (Figure 5), hydrology, and applications requiring high-resolution global topography. The basic idea is to acquire a swath of SAR data along a reference orbital trajectory and then reacquire the same image on a repeating trajectory (Figure 6). If the reference and repeat orbits are separated by less than the critical baseline (see below) then the amplitude and phase of the two images will match except for line-of-sight ground motions or changes in the surface characteristics. Spatially nonuniform motions of the surface will produce interferometric fringes (i.e., the phase difference between the two images) at a rate of one fringe per 1/2 wavelength of surface motion. Since the possible SAR wavelength ranges from a few centimeters to a meter, very small amplitude motions can be measured. Given the relatively high power and data rates available on the proposed Jupiter Icy Moons Orbiter mission (JIMO) (R. Greeley et al., Report of the NASA Science Definition Team for the Jupiter Icy Moons Orbiter, http://ossim.hq.nasa.gov/jimo/, National Aeronautics and Space Administration, Washington, D. C., 2004), it may be possible to use a synthetic aperture radar (SAR) to monitor surface deformation as well as radar wavelength-scale surface changes. Here we discuss some of the issues related to a possible InSAR mission around Europa, all of which boil down to the coherence properties of the interferometer, ultimately determining the phase fidelity and deformation acuity. These include: statistical noise characteristic of the interferometer, constraints on orbital repeat accuracy, penetration of the surface, and the number and timing of repeats needed for a definitive experiment.

[18] The first issue is thermally-induced statistical noise. The radar measurement has an intrinsic noise level that is related to the temperature and bandwidth of the instrument. Differences between the noise components of the reference and repeat pass observations cause the signals to be decorrelated. Other statistical sources of noise include quantization of the received signal and folding of energy outside the main beam of the antenna into the illuminated area of interest. To create high quality, low-noise measurements, the received signal must be significantly higher than the

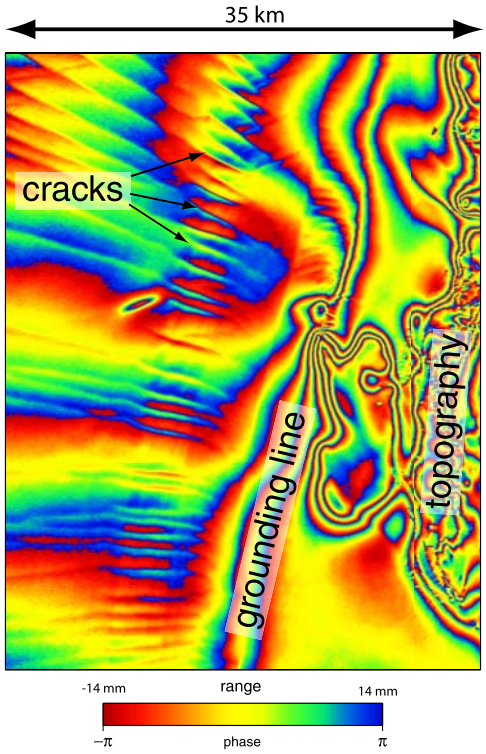

Figure 5. Example interferogram of the Amery Ice Shelf (from ERS-Tandem interferometry data), Antarctica, reveals surface changes associated with ice deformation, tides, and topography. Strain in the ice stream causes localized deformation along surface cracks. A tidal signal is apparent along the grounding line because the floating ice sheet moves vertically with the tide, while the grounded sheet does not move. Finally, because the interferometric baseline is not zero, some of the fringes are due to topography within the swath (~100 m per fringe).

noise level. The received signal level is affected by the transmitter power, antenna area, distance from the radar instrument to the surface, and the backscatter brightness of the surface. Preliminary calculations have been carried out assuming a plausible JIMO radar design within commonly accepted mission payload constraints, as given in Table 2. These calculations show that the high transmitted power levels available from a JIMO-class radar would provide sufficient signal-to-noise ratio to detect subcentimetric deformations of Europa's surface at 13 cm and 70 cm wavelengths for orbits from 100 km to 1000 km. Given the high assumed transmit power of JIMO, the principal sources of noise are quantization and ambiguities (energy-folding), not thermal effects.

[19] The second issue is to maintain phase coherence between the reference and repeat acquisitions. Coherence is highest when the reference and repeat SAR data acquisitions are coincident or at least a small fraction of the critical baseline in the moon-fixed reference frame. The critical baseline for repeat-pass interferometry is given by

$$B_c = \frac{\lambda \rho \tan\theta}{2\Delta\rho}, \tag{9}$$

where λ is the radar wavelength, ρ is the range from reference track to reflector, $\Delta\rho$ is the range resolution of radar and θ is the look angle. For a typical Earth-orbiting 5.6 cm wavelength radar (800 km altitude) the critical baseline is 1200 m so usable interferometric pairs should have baselines less than about 300 m. Figure 5 is an example of an interferogram of ice from one such radar. Since navigating a small spacecraft at Jovian distances to an accuracy of 300 m is a major technical challenge, one needs to select radar and orbital parameters that will increase the critical baseline. Table 3 highlights some of the possibilities. For example, a 13 cm-wavelength radar with 10 m resolution at an altitude of 1000 km has a critical baseline of 20 km so the repeat orbit should be navigated to within 5 km of the reference orbit good phase coherence.

[20] The third issue is the degree of penetration of the radar as a function of radar wavelength. Penetration causes the effective scattering area as seen by the radar to increase (see, e.g., volumetric decorrelation discussion by *Rosen et al.* [2000]), coarsening the effective resolution of the radar. By equation (9), this decreases the critical baseline and leads to further decorrelation and phase noise. Earth-based radar studies show that Europa has a very strong coherent backscattering behavior at radar wavelengths up to at least 13 cm [*Black et al.*, 2001]. The most likely model for this effect is cracks or suspended inclusions, which could either be voids or ice of a different refractivity, within the upper few meters of the low-loss icy crust. The coherent scattering effect appears less important at 70 cm wavelength, possibly

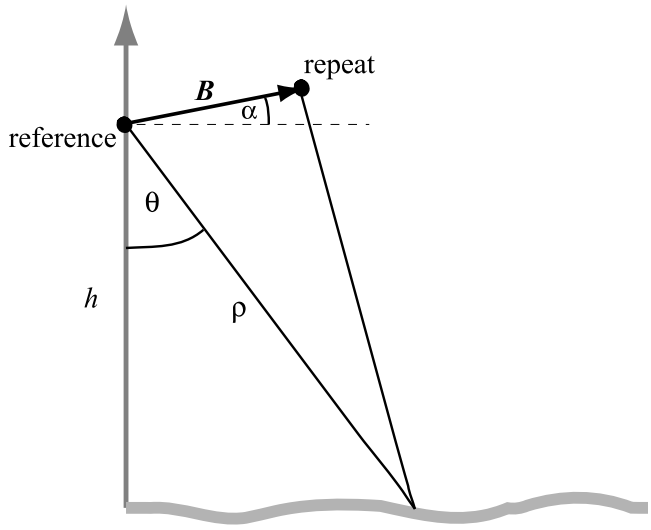

Figure 6. Geometry of repeat-pass interferometry for coherent change detection. The trajectory of the satellite orbit is into the page. The satellite is orbiting at an altitude of h on the reference orbit, and the repeat orbit is separated by a baseline of length $\boldsymbol{B}$ and angle α with respect to the horizontal. The radar is looking toward the side at an angle of θ from the vertical; ρ is the total range between the spacecraft and a pixel on the surface. The phase difference between corresponding points in the two radar images is a measure of the path length difference, which is a function of the topographic height of the surface and any displacement of the surface over the repeat interval. Ideally, for measuring change, the baseline $\boldsymbol{B}$ would be zero, such that path length differences are due purely to surface motion.

Table 2. Possible Designs for Europa SAR

Parameter	S Band	P Band
Design Parameters		
Wavelength, cm	13	70
Peak transmitter power, kW	10	10
Pulse length, μs	30	30
Pulse repetition frequency, Hz	1000	1000
Bandwidth, MHz	20	20
Antenna size, m × m	3 × 3	6 × 6
Interferometer baseline, m	1000	1000
Orbiter altitude, km	1000	1000
Look angle, degrees	25	25
Surface layer thickness, m	10	100
Image resolution, m × m	10 × 10	10 × 10
Derived Parameters		
Local incidence angle, degrees	44	44
Surface range to mid swath, km	514	514
Swath width, km	55	148
Days for global coverage (Europa)	30	11
Signal-to-noise ratio,[a] dB	14	10
Data rate, Mbps	13	16
Height error,[a] m	2	32
Displacement error,[a] mm	3	34

[a]Assumes 0 dB surface reflectivity for S band and −20 dB for P band.

due to a size limit on the cracks or suspended scattering particles. As the wavelength increases, the penetration depth increases, and the interferometric phase of the signal decorrelates because of volume scattering (nonzero baseline). The deeper penetration can be a very useful technique for mapping subsurface structure of ice sheets (as has been shown for Greenland), but may not be ideal if the goal is to study small-scale change at the surface. Therefore to avoid possible decorrelation due to volume scattering of a deeply-penetrating radar, the wavelength should be less than about 26 cm. Preliminary calculations (Table 2) of decorrelation due to penetration to a depth of 10 m at 13 cm wavelength show marginal increase in the measurement uncertainty at baselines and altitudes of interest. Penetration at 70 cm wavelength might be deeper. A scattering layer of 100 m depth at this wavelength would introduce substantial decorrelation noise (around 3 cm). Some of this noise can be mitigated by averaging neighboring pixels, at the cost of resolution.

[21] The fourth issue is the ability to repeat the ground track to within the critical baseline on at least two repeat orbits. The current scenario would place JIMO in a high inclination orbit at an altitude of 100–200 km. Achievement of full global coverage with the optical instruments will take about 14 days. Thus considering the entire Europa mission may be limited to 30 days because of the adverse effects of the severe Jovian radiation environment on the computer chips, it may only be possible to achieve two repeat cycles. For a radar with range resolution of 10 m and a wavelength of 26 cm, this will require extremely accurate spacecraft navigation (< 1000 m). The more desirable shorter-wavelength radar (13 cm) would require accuracy of better than 500 m. The unfortunate conclusion is that the short duration of the JIMO mission coupled with the high orbital navigation requirements appear to make a repeat-orbit experiment difficult.

[22] To overcome these issues of orbit control, we propose that a repeat-pass interferometry experiment be performed while the spacecraft is still spiraling into Europa to achieve the high-inclination mapping orbit. The scenario would be to interrupt the inward spiral for a few days and place the spacecraft into a circular orbit at an altitude greater than about 1000 km. At 1000 km altitude, the repeatability of the orbit can be as large as ~5000 m for a 13 cm wavelength radar (Table 3). Higher orbits will be even more accommodating to limited orbit repeatability, though eventually SNR losses will begin to limit detectability of cracks. Since the JIMO orbit tour will be studied and mutable for some time to come, for the sake of specificity we consider how the strain signal from a tidally-driven crack will appear from an altitude of 1000 km using a radar with a range resolution of 10 m and a wavelength of 0.13 m. As stated previously, interferometric performance at this altitude will be excellent. The radar should have no difficulty imaging to the limb of Europa, though observations within 10 degrees of the equator would become problematic if the orbit were equatorial.

6. Synthetic Interferograms

[23] The cracked plate model is used to generate synthetic interferograms to explore the viability and optimal characteristics of an InSAR mission at Europa. As an example Figure 7 shows surface displacement for a 256-km-long crack penetrating 0.9 of the plate thickness from the bottom-up. Both shear and normal displacement are applied on the crack using the values in Table 1 for a 10-km-thick plate. The three components of deformation are projected into a line-of-sight range change that could be observed by a SAR which acquires data during the maximum and zero of the tidal cycle. The spacecraft trajectory is at a 45° angle to the fault trace and the look angle to the ground is 35° from the vertical. We assume a 13-cm radar so one interferometric fringe will represent a range change of 6.5 cm.

[24] Assuming the parameters in Table 2, a single repeat pass pair at 13 cm wavelength would generate a strip of data of 55 km width at 10 m resolution, with 3 mm accuracy in the measurement of displacement. The synthetic displacement image has 25 cm of line-of-sight variability over spatial scale smaller than the imaging swath and much larger than the resolution limit. These deformations would be easily detected by a 13 cm wavelength repeat-pass interferometer. Even at 70 cm wavelength, the displacements are substantially larger than the 5 cm error on the measurement due to penetration. If the one were willing to

Table 3. Critical Baseline Versus Radar and Orbit Characteristics

Wavelength λ	Range Resolution Δρ	Altitude *h*, km	Critical Baseline B_c, m	Orbit Control, m
0.06	100	100	40	10
-	10	100	400	100
-	10	1000	4000	1000
0.13	100	100	200	50
-	10	100	2000	500
-	**10**	**1000**	**20000**	**5000**
0.26	100	100	400	100
-	10	100	4000	1000
-	10	1000	40000	10000

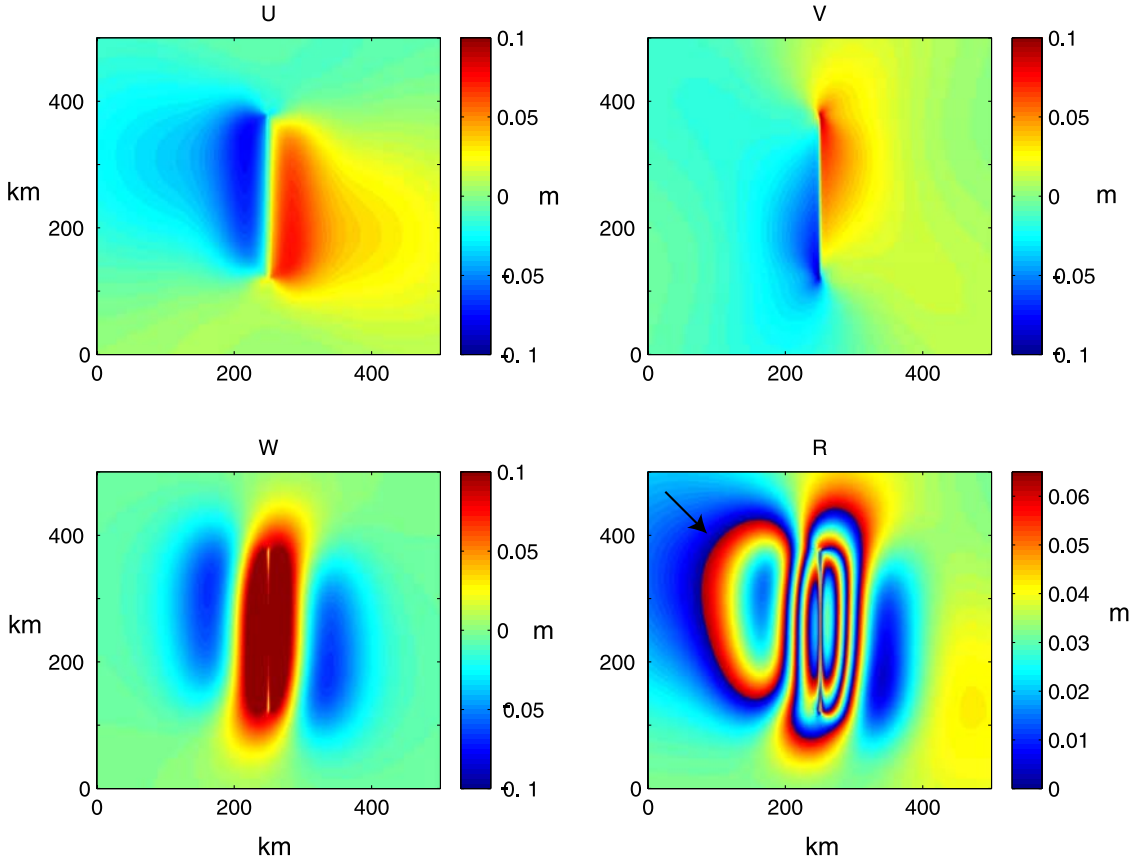

Figure 7. Surface deformation for a 10-km-thick plate with a 256-km-long crack that penetrates 0.9 of the plate thickness from the bottom. Shear and normal displacement on the crack are 0.129 m and 0.352 m, respectively (Table 1). Fault normal (U), fault, parallel (V), and vertical displacement (W) are projected into the line-of-sight (R) direction (arrow), and range is wrapped at 0.065 m to simulate an interferogram. The total line-of-sight displacement is 0.25 m or about 3.9 fringes at this radar wavelength.

sacrifice interferogram resolution to reduce noise by averaging neighboring pixels, then improved performance can be achieved. Degrading resolution would primarily limit the ability to model displacements very near the crack itself.

7. Conclusions

[25] We have investigated whether a synthetic aperture radar mission to Europa could be used to measure present-day deformation of the icy shell in areas where tidal strains are amplified above cracks. Of course, detectability depends on ratio of the surface deformation to the sensitivity of the radar interferometer. For a wide range of plate thicknesses (3–30 km) we find that surface deformation will exceed several centimeters over horizontal scales of 1–100 km if more than half of the thickness plate is fractured. Plate spreading will occur if more than 85% of the plate is fractured. Repeat-pass synthetic aperture radar could easily be used to detect and map localized tidal strain above cracks that penetrate more than half the shell thickness. As an example, an S band radar (13 cm wavelength) provides high signal-to-noise backscatter without having extreme penetration of the surface that could cause volume decorrelation. A 1000-km or higher orbital altitude is best for minimizing the requirement for real-time orbit control. It may be possible to obtain interferograms as the spacecraft spirals from its insertion altitude down to mapping altitude of 100–200 km. Two or three repeat orbits at different phases of the tide will be needed for a definitive experiment.

[26] **Acknowledgments.** We thank the members of the JIMO Science Definition Team for their insight into the generation of cracks on Europa as well as their thoughtful discussions about mission scenarios and instrumentation. The Associate Editor and reviewers provided excellent suggestions for improving the accessibility of the paper to a wider range of readers. David Sandwell was supported by NASA (NAG5-13673) and the National Science Foundation (EAR0105896). Paul Rosen and Eric Gurrola carried out the research at the Jet Propulsion Laboratory, California Institute of Technology, under a contract with NASA and were funded through the internal Research and Technology Development program. William Moore was supported by NASA (NNA04CC10A).

References

Black, G. J., D. B. Campbell, and P. D. Nicholcon (2001), Icy Galilean satellites: Modeling radar reflectivities as a coherent backscatter effect, *Icarus*, *151*, 167–180.

Blaney, D. L., and J. Spencer (2003), Jupiter Icy Moon Orbiter (JIMO) remote sensing: Geology and geochemistry science goals and objectives, *Eos Trans. AGU*, *84*(46), Fall Meet. Suppl., Abstract P11C-03.

Blankenship, D. D., D. P. Winebrenner, B. A. Campbell, R. T. Pappalardo, and D. T. Sandwell (2003), A science foundation for orbital subsurface radar sounding of Jupiter's Icy Moons, *Eos Trans. AGU*, *84*(46), Fall Meet. Suppl., Abstract P11C-04.

Brace, W. F., and D. L. Kohlstedt (1980), Limits on lithospheric stress imposed by laboratory experiments, *J. Geophys. Res.*, *85*, 6248–6252.

Buck, L., C. F. Chyba, M. Goulet, A. Smith, and P. Thomas (2002), Persistence of thin ice regions in Europa's ice crust, *Geophys. Res. Lett.*, *29*(22), 2055, doi:10.1029/2002GL016171.

Byerlee, J. D. (1978), Friction of rocks, *Pure Appl. Geophys.*, *116*, 615–626.

Carr, M. H., et al. (1998), Evidence for a subsurface ocean on Europa, *Nature*, *391*, 363–365.

Cole, D. M., and G. D. Durell (1995), The cyclic loading of saline ice, *Philos. Mag. A*, *72*, 209–229.

Crawford, G. D., and D. J. Stevenson (1988), Gas-driven water volcanism and the resurfacing of Europa, *Icarus*, *73*, 66–79.

Figueredo, P. H., F. C. Chuang, J. Rathbun, R. L. Kirk, and R. Greeley (2002), Geology and origin of Europa's "Mitten" feature (Murias Chaos), *J. Geophys. Res.*, *107*(E5), 5026, doi:10.1029/2001JE001591.

Geissler, P. E., et al. (1998), Evidence for non-synchronous rotation of Europa, *Nature*, *391*, 368–370.

Greeley, R., C. F. Chyba, J. W. Head III, T. B. McCord, W. B. McKinnon, R. T. Pappalardo, and P. Figueredo (2004), Geology of Europa, in *Jupiter: The Planet, Satellites and Magnetosphere*, Cambridge Univ. Press, New York, in press.

Greenberg, R., P. Geissler, G. Hoppa, B. R. Tufts, and D. D. Durda (1998), Tectonic processes on Europa: Tidal stresses, mechanical response, and visible features, *Icarus*, *135*, 64–78.

Greenberg, R., P. Geissler, G. Hoppa, and B. R. Tufts (2002), Tidal-tectonic processes and their implications for the character of Europa's icy crust, *Rev. Geophys.*, *40*(2), 1004, doi:10.1029/2000RG000096.

Hoppa, G., B. R. Tufts, R. Greenberg, and P. Geissler (1999a), Strike-slip faults on Europa: Global shear patterns driven by tidal stress, *Icarus*, *141*, 287–298.

Hoppa, G. V., B. R. Tufts, R. Greenberg, and P. E. Geissler (1999b), Formation of cycloidal features on Europa, *Science*, *285*, 1899–1902.

Khurana, K. K., et al. (2003), Field and plasma science with the Jupiter Icy Moons Orbiter (JIMO), *Eos Trans. AGU*, *84*(46), Fall Meet. Suppl., Abstract P11C-07.

Kivelson, M. G., K. K. Khurana, C. T. Russell, M. Volwerk, R. J. Walker, and C. Zimmer (2000), Galileo magnetometer measurements: A stronger case for a subsurface ocean at Europa, *Science*, *289*, 1340–1343.

Lee, S. W., M. Zanolin, A. M. Thode, R. T. Pappalardo, and N. C. Makris (2003), Probing Europa's interior with natural sound sources, *Icarus*, *165*(1), 144–167.

Massonnet, D., and K. Feigl (1998), Radar interferometry and its application to changes in the Earth's surface, *Rev. Geophys.*, *36*(4), 441–500.

Michalski, J. R., and R. Greeley (2002), En echelon ridge and trough structures on Europa, *Geophys. Res. Lett.*, *29*(10), 1498, doi:10.1029/2002GL014956.

Moore, W. B., and N. Makris (2003), Understanding active processes at the surfaces of Jupiter's icy moons, *Eos Trans. AGU*, *84*(46), Fall Meet. Suppl., Abstract P11C-01.

Moore, W. B., and G. Schubert (2000), The tidal response of Europa, *Icarus*, *147*, 317–319.

Nimmo, F. (2004), What is the Young's Modulus of Ice?, in *Workshop on Europa's Icy Shell: Past, Present, and Future*, pp. 7005–7006, Lunar and Planet. Inst., Houston, Tex.

Nimmo, F., B. Giese, and R. T. Pappalardo (2003), Estimates of Europa's ice shell thickness from elastically-supported topography, *Geophys. Res. Lett.*, *30*(5), 1233, doi:10.1029/2002GL016660.

Nur, A., and G. Mavco (1974), Postseismic viscoelastic rebound, *Science*, *183*(4121), 204–206.

Ojakangas, G. W., and D. J. Stevenson (1989), Thermal state of an ice shell on Europa, *Icarus*, *81*, 220–241.

Phipps Morgan, J. (1987), Mechanisms for the origin of mid-ocean ridge axial topography: Implications for the thermal and mechanical structure of accreting plate boundaries, *J. Geophys. Res.*, *92*(B12), 12,823–12,836.

Prockter, L. M., J. W. Head III, R. T. Pappalardo, R. J. Sullivan, A. E. Clifton, B. Giese, R. Wagner, and G. Neukum (2002), Morphology of Europan bands at high resolution: A mid-ocean ridge-type rift mechanism, *J. Geophys. Res.*, *107*(E5), 5028, doi:10.1029/2000JE001458.

Rosen, P. A., S. Hensley, I. R. Joughin, F. K. Li, S. S. Madsen, E. Rodriguez, and R. M. Goldstein (2000), Synthetic aperture radar interferometry, *Proc. IEEE*, *88*(3), 333–381.

Rundle, J. B., and D. D. Jackson (1977), A three-dimensional viscoelastic model of a strike slip fault, *Geophys. J. R. Astron. Soc.*, *49*, 575–591.

Rybicki, K. (1971), The elastic residual field of a very long strike-slip fault in the presence of a discontinuity, *Bull. Seismol. Soc. Am.*, *61*(1), 72–92.

Savage, J. C., and W. H. Prescott (1978), Asthenospheric readjustment and the earthquake cycle, *J. Geophys. Res.*, *83*, 3369–3376.

Smith, B., and D. T. Sandwell (2004), A three-dimensional semianalytic viscoelastic model for time-dependent analyses of the earthquake cycle, *J. Geophys. Res.*, doi:10.1029/2004JB003185, in press.

Turcotte, D. L., and G. Schubert (2002), *Geodynamics*, 2nd ed., Cambridge Univ. Press, New York.

Vaughan, D. G. (1995), Tidal flexure at ice shelf margins, *J. Geophys. Res.*, *100*, 6213–6224.

E. Gurrola and P. Rosen, Jet Propulsion Laboratory, California Institute of Technology, 4800 Oak Grove Drive, Pasadena, CA 91109, USA.

W. Moore, Department of Earth and Space Sciences, University of California, 3806 Geology Building, UCLA Box 951567, Los Angeles, CA 90095-1567, USA.

D. Sandwell, Scripps Institution of Oceanography, University of California, IGPP, Mail Code 0225, 9500 Gilman Drive, La Jolla, CA 92093-0225, USA. (dsandwell@ucsd.edu)